1040-5488/08/8509-0843/0 VOL. 85, NO. 9, PP. 843–848
OPTOMETRY AND VISION SCIENCE

ORIGINAL ARTICLE

Forward Scattering Properties of Corneal Haze

DIRK DE BROUWERE, BSc, HARILAOS GINIS, PhD, GEORGE KYMIONIS, PhD, MD, IRINI NAOUMIDI, PhD, and IOANNIS PALLIKARIS, PhD, MD

Institute of Vision and Optics, University of Crete, Heraklion, Crete, Greece (DEB, HG, IN, IP), and Bascom Palmer Eye Institute, Ft. Lauderdale, Florida (GK)

ABSTRACT

Purpose. Corneal haze is a well-known pathology associated with decreased corneal transparency and increased ocular scattering. Clinically, haze is typically estimated as the amount of backscattered light observed in a slit lamp examination while the small angle forward scattering cannot be directly observed. It was the purpose of this study to demonstrate a single-pass technique to objectively measure forward scattering properties of excised rabbit corneas.

Methods. Six rabbits (twelve eyes) were used in this study. All eyes underwent photorefractive keratectomy for −4 D in a 6 mm ablation zone. Seven weeks later, the rabbits were examined under general anesthesia. All eyes expressed mild to severe haze. A purposely-developed single pass optical setup was used both to estimate the angular distribution and fraction of forward light scattering in excised rabbit corneas. Moreover, subjective clinical corneal haze evaluation was performed as well as corneal confocal microscopy of all corneas. Finally, the corneas were histopathologically examined.

Results. Light scattering in the rabbit corneas followed a narrow forward peaked distribution. A new parameter, Ballistic Ratio, was introduced to represent a parameter for absolute quantification of forward light scatter, corresponding to the power ratio of the radiation that is not scattered by each sample. A negative correlation between clinically subjective corneal haze and forward scatter (Pearson's Coefficient = −0.23) was found, which suggests the relation between increased forward and backward scatter. Activated myofibroblasts, collagen irregularities and vacuoles present in a sub-epithelial layer over the treated area of the cornea had characteristic dimensions in accordance to the measured scatter distribution.

Conclusions. Corneal light scatter associated with the increased amount of haze after excimer laser ablation has a narrowly forward distribution that can be attributed to the subepithelial structures observed in treated corneas.
(Optom Vis Sci 2008;85:843–848)

Key Words: haze, scattering, PRK, keratocytes, cornea

Corneal haze is a potential complication of refractive surgery especially after surface ablations.[1,2] It is a well known pathology associated with increased ocular scattering. Clinically haze is typically estimated as the amount of backscattered light observed in a slit lamp examination. During slit lamp examination, the backscattered light is assessed, whereas the small angle forward scattered light (mainly affecting retinal image quality) cannot be observed.

Several theories pertaining to the origin of corneal scatter have been suggested. Hart and Farrell associated the high degree of corneal transparency to the organized packing of the stromal collagen layers.[3] They simulated the diffraction on a structure of regularly packed arrays and concluded that light only constructively interferes in the direction of propagation. Furthermore, Van den Berg et al. simulated a close similarity with the ciliary corona using a model of interference between small scattering particles in the ocular media.[4]

It has been proposed that irregular packing of the stromal collagen layers, discontinuities in the epithelium-stromal interface, and corneal edema/fibroblasts activated during the wound healing process, plays a role in the corneal haze development,[5,6,7] which is associated with increased light scatter.[8,9] However, haze is clinically observed as the estimation of backscattered light. The small angle forward distribution of light scatter in corneas expressing different grades of haze has not been yet investigated.[10]

Based on observations in confocal microscopy (CFM),[5] we propose a scattering distribution based on small particle scattering.[11] Assuming that the cornea is a partially scattering layer, a portion of the incoming light will be scattered following the angular distribution of the scattering law. The other portion follows the regular refractive path of the ocular optics focusing on the retina. In our model, we restricted scattering particles to the highly reflective objects found in CFM, namely

activated keratocytes and other extracellular reflective structures of similar dimensions.[12]

The purpose of this study was to employ a single-pass optical method to estimate corneal transparency in excised rabbit corneas following laser ablation, to measure the forward scattering distribution for angles smaller than 2° and to quantify corneal scatter by means of a power parameter, the Ballistic Ratio (BR). Moreover, to correlate these findings with clinically observed haze and histological findings.

MATERIALS AND METHODS

Animal Treatment

Twelve eyes of six pigmented adult male rabbits, weighting 2.5 to 3.5 kg were used in the study. The animals were treated in accordance to the guidelines of the Association for Research and Vision in Ophthalmology Statement for the Use of Animals in Ophthalmic and Vision Research.

For surgery (photorefractive keratectomy), the animals were anesthetized by an intramuscular injection of a mixture of xylazin hydrochloride (5 mg/kg) and ketamine hydrochloride (50 mg/kg). An eyelid speculum was introduced and two drops of topical anesthesia (sodium chloride proxymetacain, Alcaine, ALCON Lab, Hellas AEBE) were instilled. Two minutes after topical corneal anesthesia, mechanical epithelium debridement of the central 6 mm of the cornea (previously marked with a 6 mm trephine) was performed with a brush followed by a myopic photoablation performed using a 193 nm Excimer laser (Wavelight Allegretto 400 Erlangen, Germany) operating at an average fluence of 180 mJ/cm^2 per pulse and a repetition rate of 400 Hz. The ablation pattern delivered to all eyes was programmed for −4 D at an optical zone of 6 mm, removing approximately 49 μm of stromal tissue in the center of the ablation zone. Antibiotic ointment (Tobramycin 0.3%) was administered to all eye four times daily until re-epithelialization was complete. As the purpose of this study was to evaluate corneal haze, no topical steroids were applied since their action would minimize haze formation.

Postoperative Examinations and Histopathological Evaluation

Seven weeks after treatment, all eyes were evaluated for haze by means of slit lamp examination by a refractive surgeon (GDK). All corneas were evaluated by HRTII (Heidelberg Engineering, Germany) CFM before surgery, and at weeks 1, 2, 3, and 7 after surgery. Immediately after the CFM imaging on week 7, all animals were sacrificed and eyes were enucleated. To maintain normal hydration conditions, corneas were excised along with a 2 mm scleral rim. Forward scattering was assessed using a single-pass device presented in the following paragraph. Finally, all corneas were prepared for histologic examination (light microscopy) by trichrom staining. Histological fixation of all specimens (with glutaric aldehyde) was made within 5 min after enucleation.

Optical Setup for the Measurement of Single Pass Forward Scatter

A purposely-constructed optical setup was employed for the evaluation of narrow-angle forward scattering. The setup is illustrated in Fig. 1.

The setup involved a Charge-Coupled Device (CCD) camera (Sony XCD-X700) using a custom-made camera lens and two different light sources serving as objects. The camera lens consisted of one plano-convex and one plano-concave element. The refractive surfaces of the lenses had curvatures similar to the anterior and posterior curvatures of the rabbit cornea, respectively. The excised cornea occupied the space between the lenses. Carbomer gel 0.3% (Thilogel, ALCON Hellas AEBE) was used to facilitate optical contact between these three elements. An additional plano-convex lens (also optically coupled with carbomer gel) was used to adjust the total dioptric power of the camera lens to approximately 35 D. All lenses were aligned using a custom-made lens mount that ensured that the optical elements were properly centered. Although optical aberrations were not measured, ZEMAX simulations (ZEMAX Development Corporation Bellevue, WA) predicted that the objective would be relatively sensitive on tilt. To minimize the impact of aberrations a 2 mm diaphragm was introduced in front of the lens.

For each cornea, a point source (back-illuminated 500 um pinhole) was imaged through the camera objective. Each image was constructed by adding two separate images acquired using two different exposure times. The first image (short exposure) was used to image the intensity of the point source itself where as the second (long exposure) was used to image the scattered light. Each image was corrected according to the camera's gamma function (deter-

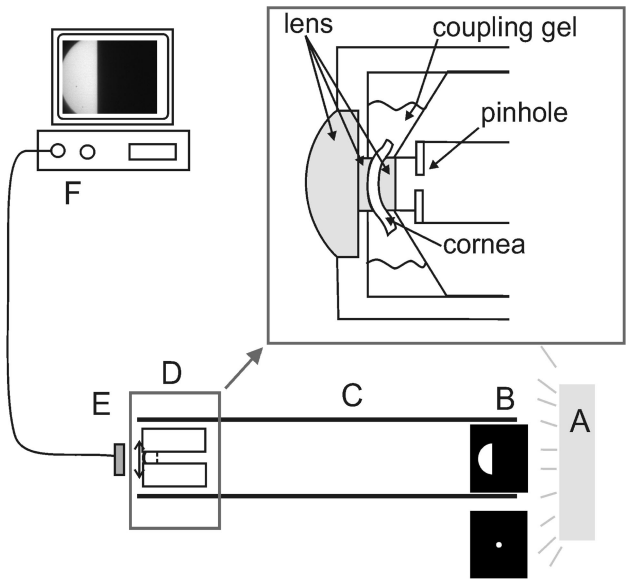

FIGURE 1.

Experimental setup. Down and left upper corner: Pi-by-no imaging setup. Images of the point source and semi-disk (B) on the CCD plane are displayed and analyzed on a PC. In the right upper corner, a detail of the camera objective is shown. The cornea was immersed in carbomer gel and enclosed between two lenses with the same curvature as the cornea. A 2 mm pinhole in front of the lens system was inserted to reduce the effect of aberrations.

mined in a separate experiment), and finally the two separate images were registered and the saturated pixels of the long exposure image were substituted by the corresponding pixels in the short exposure image (multiplied by the ratio of the exposure times). This technique allowed us to effectively extend the dynamic range of the camera by a factor 100. The compound image for each cornea was used to estimate the angular distribution of scattered light (see Results section "Estimation of Scattering Distribution").

In addition, a uniform illumination semi-disk was imaged using each cornea. The exposure time was controlled in order to utilize the full dynamic range of the camera. The images acquired using the semi-disk were used to calculate the power ratio of scattered light.

Introducing a parameter for absolute quantification of scatter, we define BR as the portion of the light passing the scattering layer not scattered on its refractive path to the retina as:

$$BR = \frac{E_{nonscattered}}{E_{scattered} + E_{nonscattered}} \quad (1)$$

where $E_{nonscattered}$ and $E_{scattered}$ are the energies (within the exposure time) corresponding to directional (non-scattered) and forward scattered light, respectively. Discrimination of these energies by image analysis of point sources is inherently difficult due to the small intensity of the forward scattered light (in respect to directional light) and errors associated to noise.

The imaging of an extended source (such as the semi-disk) is justified when the following considerations are taken into account.

Light distribution of a point imaged through the scattering surface is a weighted sum of two distributions. A part, proportional to BR follows the light distribution according to diffraction and wavefront errors of the optical system. The other part of the light, proportional to 1-BR, distributes the light according to the angular distribution of scatter.

$$PSF_{total} = BR\ PSF_{optical} + (1-BR)\ PSF_{scatter} * PSF_{optical} \quad (2)$$

Assuming that the $PSF_{optical}$ has significantly smaller dimensions than the $PSF_{scatter}$, the equation above becomes:

$$PSF_{total} \approx BR\ PSF_{optical} + (1-BR)\ PSF_{scatter} \quad (3)$$

When an extended source is imaged, the resulting image is a weighted superposition of the original image (blurred with the optical PSF) and the convolution of the blurred image with a function as described in Eq. 3.

Typically, in the case of point source imaging, the intensity of scattered light on the image plane is several orders of magnitude smaller than the intensity of the directional light. Therefore, it is difficult to observe and accurately quantify the amount of scattered light in an image of a point source. Utilizing extended sources may result to an image of lower dynamic range, with intensities of scattered light that are relatively higher and therefore easier to measure.

Image Acquisition and Processing

A semi-disk was formed by a translucent disk with a radius of 2.7° occluded by a knife-edge through the center of the disk. The object was back-illuminated with a uniform white light source. Initially, a simulated image was generated, convolving the semi-disk with the 2 mm diffraction limited point spread function.

This simulated image corresponds to the image on the CCD in absence of scatter. Further, it was convolved with the scattering PSF determined experimentally (see Results section, "Estimation of Scattering Distribution"). This simulated image corresponds to the image on the CCD if each photon was scattered exactly once. Following Eq. 3, a set of 100 calculated images was generated as a weighted sum of the above-mentioned scattered and not-scattered simulated images for varying BR from 0.01 to 1.

The experimentally acquired semi-disk images (through each cornea) were cropped to a rectangle in the occluded field starting at the knife-edge border and averaged across the direction perpendicular to the edge. Like this, 2-degree step response was calculated starting from the knife-edge towards the periphery of the occluded field. This response was compared with the response of the simulated images previously described. The value of BR used in the simulated image that best matched the experimental image [minimum root mean square (RMS) difference] was used to characterize each cornea. All analysis and simulation was done in Matlab (The Mathworks, Inc.)

RESULTS

Estimation of Scattering Distribution

Fig. 2a shows the image of the point source through four different corneas with different amounts of scatter. The central portion of the image (involving the directional light) is saturated. In all images, exposure was identical and adjusted to visualize the glare and the fine needles originating from the center and slowly disappearing towards the periphery. These needles correspond closely to the ciliary corona as proposed by van den Berg et al.[4] This model was based on light interference on scattered light generated by small particles. In our study, we applied a simplified model of non-coherent light scattering from small particles, namely the anomalous diffraction approximation of Mie scattering.[11] In this approximation, all scatterers are modeled as perfect spheres with a given radius and refractive index. As the variation of particle sizes has a much bigger impact on the scattering distribution than the wavelength, we simulated the scattering PSF using a wavelength of 600 nm. The scattering model takes into account the ratio of the refractive index of the spheres to the refractive index of the background matrix and the particle size. These parameters were initially set based on the corneal stroma irregularities (fibroblasts, and other reflective structures) that were observed using CFM.

Following an initial estimation of the forward scatter distribution based on images of point sources (Fig. 3), the average size, BR and refractive index of the particles were optimized in order to reproduce the scatter function obtained experimentally from the semi-disk images. Optimization was performed by minimizing the RMS difference between the model and the experimental semi-disk images in a field of 2° around the edge of the disk. Optimal fit was obtained for a particle size distribution of 36.7 ± 15 um and a relative refractive index of 1.0024. The fit obtained is shown in Fig. 2b.

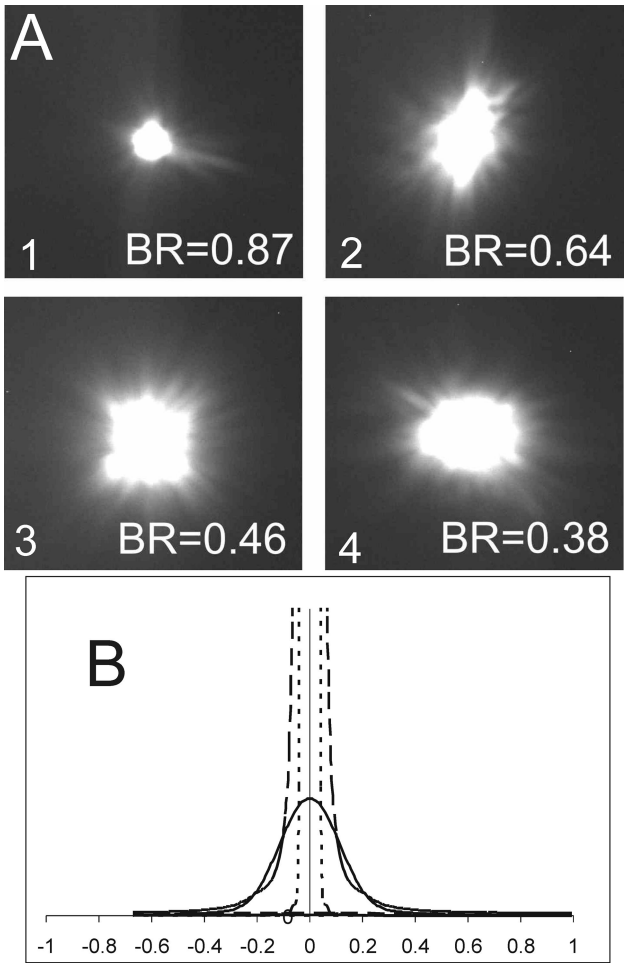

FIGURE 2.

Images of scattering PSF for different levels of scattering (BR). Field: 2 × 2° (a). Radial averaged profile of computed and measured PSF. Dashed line: average of all measured images, Dotted line: Radial profile for diffraction limited PSF (directional light), full line: Radial profile of Scattering Distribution (all scattered light) (b) Horizontal axis is degrees.

Correlation of BR with Clinical Haze

Corneal haze—as observed clinically—was graded according to a scale proposed by Fantes et al.[13] This haze parameter ranges from 0 (no haze) to 4 (severe haze). All eyes were assessed by the same investigator immediately before the animals were sacrificed. The calculated BR for each cornea is plotted against the subjective haze grade in Fig. 3. A negative correlation between these parameters (Pearson's Coefficient = −0.23) was found suggesting the relation between increased forward and backward (clinically observed) light scatter (haze). This finding suggests that corneas characterized by increased forward scatter tend to express higher clinical haze.

Correlation of BR with Histological Evaluation

Histology was performed on all eyes at week 7. Representative structures observed on the stained samples are shown in Fig. 4. The main histological finding in all eyes was subepithelial scar tissue, which had also observed in CFM. However, histology sections allowed the examination of larger areas on the cornea. The scar tissue consisting of both newly formed and unorganized collagen and activated keratocytes seems critical for the development of corneal scatter postoperatively.

Based on approximately 10 pictures for each corneal sample, the relative thickness of the scar tissue layer was measured. The relative thickness of the scar tissue was correlated (Pearson's coefficient =

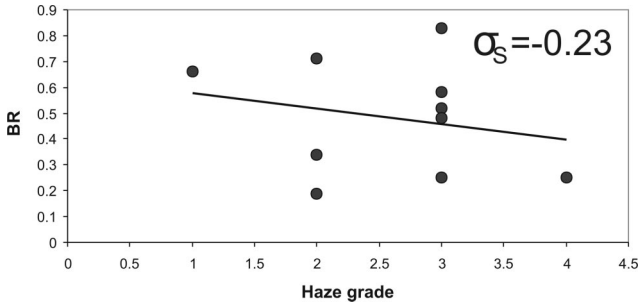

FIGURE 3.

Comparison of BR with haze grade. Note that all eyes had a high haze grade.

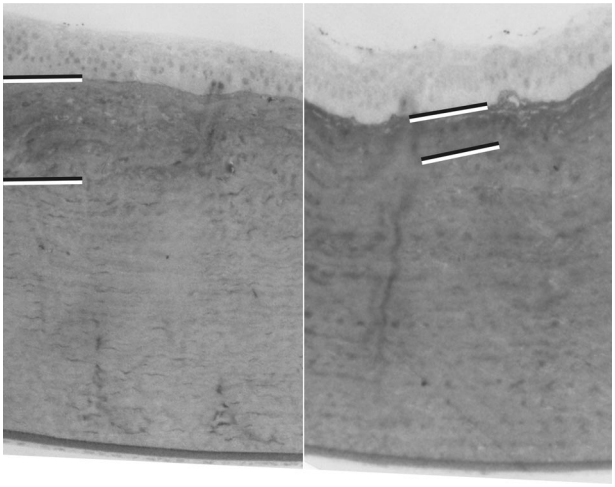

FIGURE 4.

Representative images of histological analysis. Different thicknesses of the scar tissue are indicated.

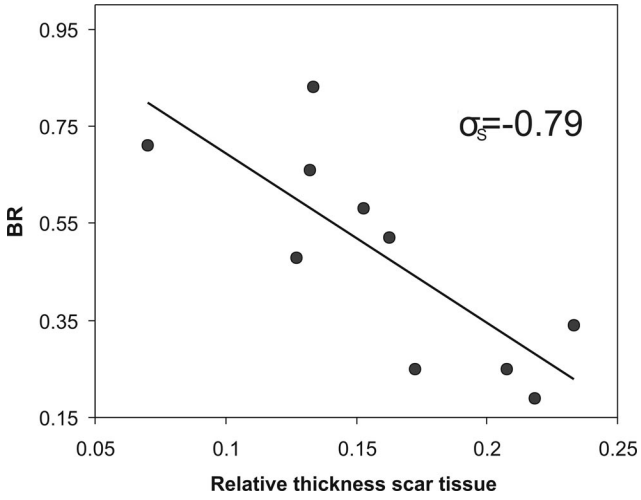

FIGURE 5.

Comparison between BR and relative thickness of scar tissue.

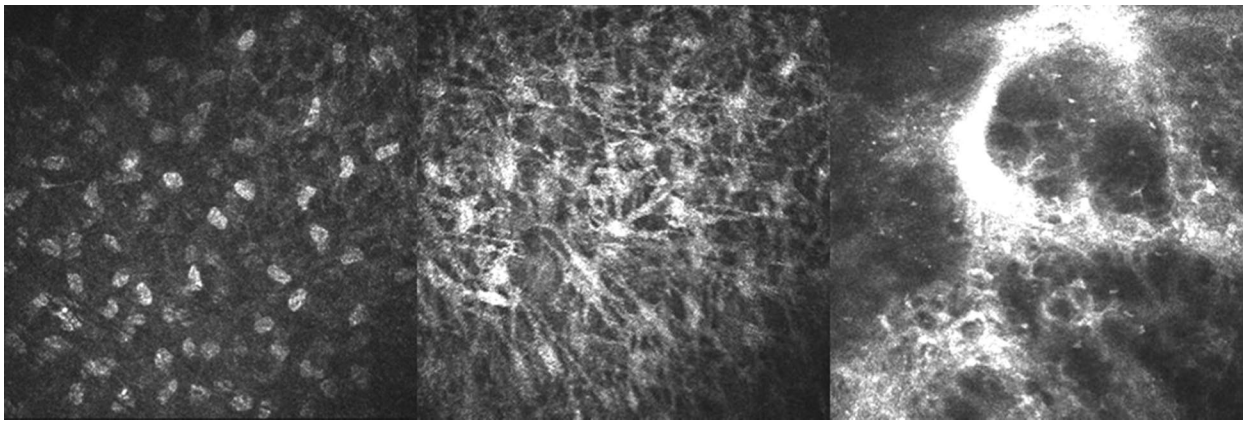

FIGURE 6.

Confocal images of anterior stromal layer (HRTII Rostock Corneal Module, Heidelberg Engineering), field: 400 × 400 um. Left: Preop image, keratocytes. Center: 7 week post op, reflective keratocytes. Right: 7 weeks post op, unorganized reflective patches.

−0.79) to the BR previously estimated for each sample. This finding suggests that a thicker scar tissue layer results to increased forward light scattering (lower BR) (Fig. 5).

Two corneas were excluded from this analysis as no suitable histological photographs could be obtained.

DISCUSSION

Our results suggest that the intensity distribution of scattered light on the cornea is characterized by a narrow forward distribution. Several scattering models can be applied to approach the obtained experimental distribution. We optimized a model based on scattering on small spherical particles, varying the size distribution of the scattering spheres to match the scattering distribution with our experimental findings. Since we were interested in quantitative measurements of forward light scattering, optimization of other free parameters in the model, such as relative refractive index and spectral distribution, were out of the scope for this study. However, the characteristic size of the scatterers in our model (36.7 ± 15 um) reproducing the experimental scatter distribution for polychromatic light, suggests that the main cause of scattering in the postablation cornea is the subepithelial region, characterized also by irregularities of that scale. The irregularities in this region (typically 50 μm deep) are extracellular reflective structures[5,6,14,15,16] characteristic of scar tissue. The hypothesis that this layer is the main cause of scatter is further supported by the strong correlation of its thickness with the calculated BR and subjective haze.

Our analysis was performed based on measurements made 7 weeks after the treatment, since it has been reported[12] that at about this postoperative time interval activation of keratocytes reaches a maximum, and the highest haze grade[5] is observed. On a long-term study, haze drops rapidly between 3 and 6 mo to decrease slowly further after 1 year.[17] Though there is no significant increase of haze a year after surgery, collagen irregularities, remaining in the stroma, can give rise to steady state of increased scatter.

Apparently, reflective structures observed using the confocal microscope contributed also to macroscopic (clinical) backscatter. Most of these reflective structures were observed in the subepithelial stroma suggesting that they possibly correspond to newly formed scar tissue.[5,18] Fig. 6 shows three different images of these reflective structures. Since highly reflective structures in CFM correspond to an abrupt change in the refractive index, it is reasonable to hypothesize that these structures play a key role in corneal scattering.

The images acquired using the CFM correspond to a small portion of the cornea (400 × 400 μm). Given the variability of the size and appearance of the irregularities across the cornea, it was difficult to select and grade CFM images for quantitative analysis. Moreover, newly formed collagen represents healing activity that could compromise the accuracy of refractive corrections.[5]

The correlation between backscattered light as estimated in the slitlamp examination (subjective haze) and forward scattered light as quantified with BR is a reasonable finding as it is related to the density of scatterers. The negative sign of the correlation originates from the fact that increasing BR corresponds to more clear corneas where as increased haze corresponds to less clear corneas. However, it needs to be pointed out that forward scattered light is more intense than backscattered light, therefore the patient may experience the effects of straylight even when the corneal seems clear in the clinical examination. It is suggested that postoperative pharmaceutical treatments should target the formation of this scar tissue to preserve corneal transparency.

ACKNOWLEDGMENTS

This work was supported by the European Training Network "Sharp-Eye".
Received September 21, 2007; accepted March 12, 2008.

REFERENCES

1. Chang SS, Maurice DM, Ramirez-Florez S. Quantitative measurement of corneal haze after myopic PRK. J Refract Surg 1996;12: 412–6.
2. Lohmann CP, Gartry DS, Muir MK, Timberlake GT, Fitzke FW, Marshall J. Corneal haze after excimer laser refractive surgery: objective measurements and functional implications. Eur J Ophthalmol 1991;1:173–80.
3. Hart RW, Farrell RA. Light scattering in the cornea. J Opt Soc Am 1969;59:766–74.
4. van den Berg TJ, Hagenouw MP, Coppens JE. The ciliary corona:

physical model and simulation of the fine needles radiating from point light sources. Invest Ophthalmol Vis Sci 2005;46:2627–32.
5. Moller-Pedersen T, Cavanagh HD, Petroll WM, Jester JV. Stromal wound healing explains refractive instability and haze development after photorefractive keratectomy: a 1-year confocal microscopic study. Ophthalmology 2000;107:1235–45.
6. Meek KM, Leonard DW, Connon CJ, Dennis S, Khan S. Transparency, swelling and scarring in the corneal stroma. Eye 2003;17: 927–36.
7. Moller-Pedersen T. Keratocyte reflectivity and corneal haze. Exp Eye Res 2004;78:553–60.
8. Ivarsen A, Laurberg T, Moller-Pedersen T. Role of keratocyte loss on corneal wound repair after LASIK. Invest Ophthalmol Vis Sci 2004; 45:3499–506.
9. Soya K, Amano S, Oshika T. Quantification of simulated corneal haze by measuring back-scattered light. Ophthalmic Res 2002;34: 380–8.
10. Hemenger RP. Small-angle intraocular light scatter: a hypothesis concerning its source. J Opt Soc Am A 1988;5:577–82.
11. van de Hulst HC. Light Scattering by Small Particles. New York, NY: Dover Publications; 1981.
12. Perez-Gomez I, Efron N. Change to corneal morphology after refractive surgery (myopic laser in situ keratomileusis) as viewed with a confocal microscope. Optom Vis Sci 2003;80:690–7.
13. Fantes FE, Hanna KD, Waring GO, III, Pouliquen Y, Thompson KP, Savoldelli M. Wound healing after excimer laser keratomileusis (photorefractive keratectomy) in monkeys. Arch Ophthalmol 1990; 108:665–75.
14. Bohnke M, Thaer A, Schipper I. Confocal microscopy reveals persisting stromal changes after myopic photorefractive keratectomy in zero haze corneas. Br J Ophthalmol 1998;82:1393–400.
15. Böhnke M, Thaer A, Schipper I. Confocal microscopy reveals persisting stromal changes after myopic photorefractive keratectomy in zero haze corneas. Br J Ophthalmol1998; 82:1393–400.
16. Hanna KD, Pouliquen Y, Waring GO, III, Savoldelli M, Cotter J, Morton K, Menasche M. Corneal stromal wound healing in rabbits after 193-nm excimer laser surface ablation. Arch Ophthalmol 1989; 107:895–901.
17. Rajan MS, Jaycock P, O'Brart D, Nystrom HH, Marshall J. A long-term study of photorefractive keratectomy; 12-year follow-up. Ophthalmology 2004;111:1813–24.
18. Dawson DG, Edelhauser HF, Grossniklaus HE. Long-term histopathologic findings in human corneal wounds after refractive surgical procedures. Am J Ophthalmol 2005;139:168–78.

Dirk De Brouwere
Institute of Vision and Optics
University of Crete
GR-71103 Voutes Heraklion
Crete, Greece
e-mail: debrouwere@med.uoc.gr